NF-κB inhibition delays DNA damage–induced senescence and aging in mice

Jeremy S. Tilstra,[1] Andria R. Robinson,[2,3] Jin Wang,[4] Siobhán Q. Gregg,[3,5] Cheryl L. Clauson,[1] Daniel P. Reay,[6] Luigi A. Nasto,[7] Claudette M. St Croix,[8] Arvydas Usas,[7] Nam Vo,[7] Johnny Huard,[1,7] Paula R. Clemens,[6] Donna B. Stolz,[5] Denis C. Guttridge,[9] Simon C. Watkins,[5] George A. Garinis,[10] Yinsheng Wang,[4] Laura J. Niedernhofer,[1,3] and Paul D. Robbins[1,7]

[1]Department of Microbiology and Molecular Genetics, University of Pittsburgh School of Medicine, Pittsburgh, Pennsylvania, USA. [2]Department of Human Genetics, University of Pittsburgh Graduate School of Public Health, Pittsburgh, Pennsylvania, USA. [3]University of Pittsburgh Cancer Institute, Pittsburgh, Pennsylvania, USA. [4]Department of Chemistry, University of California, Riverside, California, USA. [5]Department of Cell Biology, University of Pittsburgh School of Medicine, Pittsburgh, Pennsylvania, USA. [6]Department of Neurology, University of Pittsburgh School of Medicine and Neurology Service, Department of Veterans Affairs Medical Center, Pittsburgh, Pennsylvania, USA. [7]Department of Orthopaedic Surgery and [8]Department of Environmental and Occupational Health, University of Pittsburgh School of Medicine, Pittsburgh, Pennsylvania, USA. [9]Department of Molecular Virology, Immunology and Medical Genetics, The Ohio State University, Columbus, Ohio, USA. [10]Institute of Molecular Biology and Biotechnology-FORTH, Heraklion, Greece.

The accumulation of cellular damage, including DNA damage, is thought to contribute to aging-related degenerative changes, but how damage drives aging is unknown. XFE progeroid syndrome is a disease of accelerated aging caused by a defect in DNA repair. NF-κB, a transcription factor activated by cellular damage and stress, has increased activity with aging and aging-related chronic diseases. To determine whether NF-κB drives aging in response to the accumulation of spontaneous, endogenous DNA damage, we measured the activation of NF-κB in WT and progeroid model mice. As both WT and progeroid mice aged, NF-κB was activated stochastically in a variety of cell types. Genetic depletion of one allele of the p65 subunit of NF-κB or treatment with a pharmacological inhibitor of the NF-κB–activating kinase, IKK, delayed the age-related symptoms and pathologies of progeroid mice. Additionally, inhibition of NF-κB reduced oxidative DNA damage and stress and delayed cellular senescence. These results indicate that the mechanism by which DNA damage drives aging is due in part to NF-κB activation. IKK/NF-κB inhibitors are sufficient to attenuate this damage and could provide clinical benefit for degenerative changes associated with accelerated aging disorders and normal aging.

Introduction

Aging is characterized by the inability of tissues to maintain homeostasis (1, 2). This leads to an impaired response to stress and, as a consequence, an increased risk of morbidity and mortality (2). The incidence of numerous debilitating chronic diseases, such as cardiovascular disease, neurodegeneration, diabetes, arthritis, and osteoporosis, increases almost exponentially with age (3). Aging is thought to be driven, at least in part, by the accumulation of stochastic damage in cells. This includes damage to proteins (2), DNA, mitochondria (4), and telomeres (5), which is driven by ROS (6–8) generated through chronic inflammation (9, 10) or aerobic respiration in mitochondria (4). However, the mechanism by which cellular damage drives aging is not known. The simplest model is that damage causes attrition of functional cells. But this is inadequate in light of emerging evidence that aging-related degenerative changes in old and damaged organisms can be delayed or reversed by circulating factors (11–15). These observations point instead toward the cellular response to damage being the key driver of aging.

The transcription factor NF-κB is a central component of the cellular response to damage, stress, and inflammation (16). In mammals, the NF-κB family consists of 5 subunits, RelA or p65, c-Rel, RelB, p50, and p52. NF-κB binds to DNA as a dimer, the most common being the p65p50 heterodimer (17). The p65p50 heterodimer is localized primarily in the cytoplasm, maintained in this inactive state via sequestration by IκB proteins (17). NF-κB activation via the canonical pathway is mediated by the upstream IκB kinase (IKK), a heterotrimer consisting of 2 catalytic subunits, IKKα and IKKβ, and a regulatory subunit termed IKKγ or NF-κB essential modulator (NEMO) (17). In response to a variety of factors, including proinflammatory cytokines, pathogens, oxidative stress, and growth factors, IKK is activated and phosphorylates IκB, leading to its polyubiquitination and subsequent proteasomal degradation (16, 18–20). IκB degradation allows NF-κB to translocate to the nucleus, in which it binds to its cognate DNA sequence as well as coactivators, such as CBP/p300, to regulate gene expression (21).

Numerous studies report increased NF-κB activity with aging. Human fibroblasts from aged individuals and patients with Hutchinson-Gilford progeria syndrome have increased NF-κB activation (22, 23). NF-κB DNA binding is increased in skin, liver, kidney, cerebellum, cardiac muscle, and gastric mucosa of old rodents compared with that in young rodents (24–28). In addition, NF-κB was identified as the transcription factor most associated with mammalian aging, based on patterns of gene expression (23). Furthermore, chronic activation of NF-κB is observed in numerous age-related diseases (29), including muscle atrophy (30, 31), multiple sclerosis (32), atherosclerosis (33), heart disease (34), both type 1 and 2 diabetes (35), osteoarthritis (36), dementia (37), osteoporosis (38), and cancer (39). However, these studies do not demonstrate a causal relationship between NF-κB activation and aging.

Authorship note: Jeremy S. Tilstra, Andria R. Robinson, Jin Wang, Siobhán Q. Gregg, and Cheryl L. Clauson contributed equally to this work.

Conflict of interest: The authors have declared that no conflict of interest exists.

Citation for this article: *J Clin Invest.* 2012;122(7):2601–2612. doi:10.1172/JCI45785.

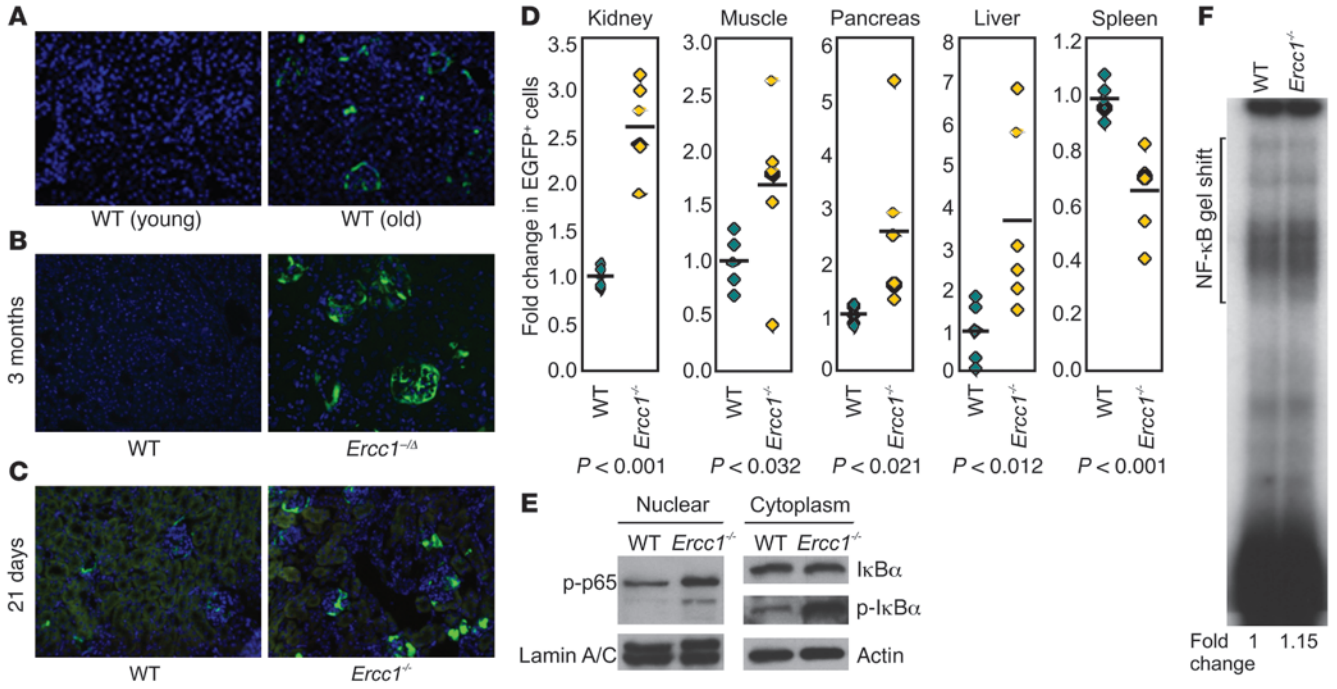

Figure 1

NF-κB activation is increased in tissues of old WT and progeroid, DNA repair–deficient mice. Kidney sections from NF-κB^{EGFP} mice were imaged using fluorescent microscopy to detect EGFP expression (green). Nuclei were counterstained with Hoechst dye (blue; original magnification, ×20). (**A**) Young adult (3-month-old) and old WT NF-κB^{EGFP} (2-year-old) mice. (**B**) *Ercc1*$^{-/\Delta}$NF-κB^{EGFP} and WT NF-κB^{EGFP} mice at 3 months of age. (**C**) *Ercc1*$^{-/-}$NF-κB^{EGFP} and WT NF-κB^{EGFP} mice at 21 days of age. (**D**) Quantification of EGFP expression. The number of EGFP^{+} cells was counted in 5 random fields of tissue per mouse (n = 6 mice per group). The fold difference in the number of EGFP^{+} cells relative to the mean value (black bar) of the group is reported. Diamond symbols represent individual mice (controls in green and *Ercc1*$^{-/-}$NF-κB^{EGFP} mice in yellow). P values were calculated using a Student's t test. (**E**) *Ercc1*$^{-/-}$ and WT primary MEFs were passaged 5 times at 20% O_2 to promote the onset of senescence (58). The levels of p-p65, IκBα, and p-IκBα in nuclear and cytoplasmic extracts were measured by immunoblot. (**F**) NF-κB EMSA was performed with a radiolabeled oligonucleotide containing an NF-κB binding site using nuclear extracts from *Ercc1*$^{-/-}$ and WT primary MEFs.

Genetic depletion of NF-κB in the skin of transgenic mice reversed age-related gene expression and histologic changes (23), providing support for NF-κB activation playing a causal role in skin aging. Similarly, haploinsufficiency of p65 leads to improved growth and extended life span of *Sirt6*$^{-/-}$ mice (40). However, *Sirt6*$^{-/-}$ mice manifest severe colitis, suggesting that chronic inflammation may drive their degenerative phenotypes and that attenuating this inflammation through genetic depletion of NF-κB accounts for their improved life span (41, 42). Thus, it remains to be determined whether NF-κB activation drives systemic aging and whether NF-κB is a therapeutic target for attenuating and/or delaying aging-related degenerative changes.

To address these gaps in knowledge, we used a mouse model of XFE progeroid syndrome, a disease of accelerated aging caused by mutations in *XPF*, which encodes the catalytic subunit of the xeroderma pigmentosum group F–excision repair cross-complementing rodent repair deficiency complementation group 1 (XPF-ERCC1) DNA repair endonuclease. The syndrome is characterized by accelerated aging of virtually all organ systems, all driven by failure to repair stochastic endogenous DNA damage. A murine model of XFE progeroid syndrome, *Ercc1*$^{-/\Delta}$ mice, have about 10% of the normal amount of ERCC1 protein and spontaneously develop progressive, degenerative changes that correlate strongly with natural aging (43–47). Thus, *Ercc1*$^{-/-}$ mice, which have a complete absence of ERCC1 protein, and *Ercc1*$^{-/\Delta}$ mice offer a unique opportunity to investigate the mechanism by which one type of cellular damage promotes aging and whether NF-κB plays a pivotal role.

We found that NF-κB is stochastically activated in a variety of cell types with normal and accelerated aging and that genetic or pharmacologic inhibition of NF-κB activation delays the onset of numerous aging-related symptoms and pathologies. Inhibition of IKK/NF-κB activity reduced cellular senescence and oxidative damage, including DNA and protein damage, revealing that cellular stress responses promote further cellular damage. Our findings strongly suggest that inhibitors of the IKK/NF-κB pathway may delay damage and extend healthspan in patients with accelerated aging and chronic degenerative diseases of old age.

Results

NF-κB is activated during normal and accelerated aging. To examine the extent of NF-κB activation associated with aging, NF-κB^{EGFP} knockin mice, with the EGFP reporter under the control of NF-κB regulatory elements (NF-κB^{EGFP}), were used (48). Kidney specimens from 3-month-old and 2-year-old NF-κB^{EGFP} reporter mice were compared (Figure 1A). The older WT mice had more cells expressing EGFP compared with young WT mice, indicative of increased NF-κB activation. EGFP expression was observed primarily in the glomeruli and was stochastic, with many cells showing strong expression while neighboring cells showed none. To determine

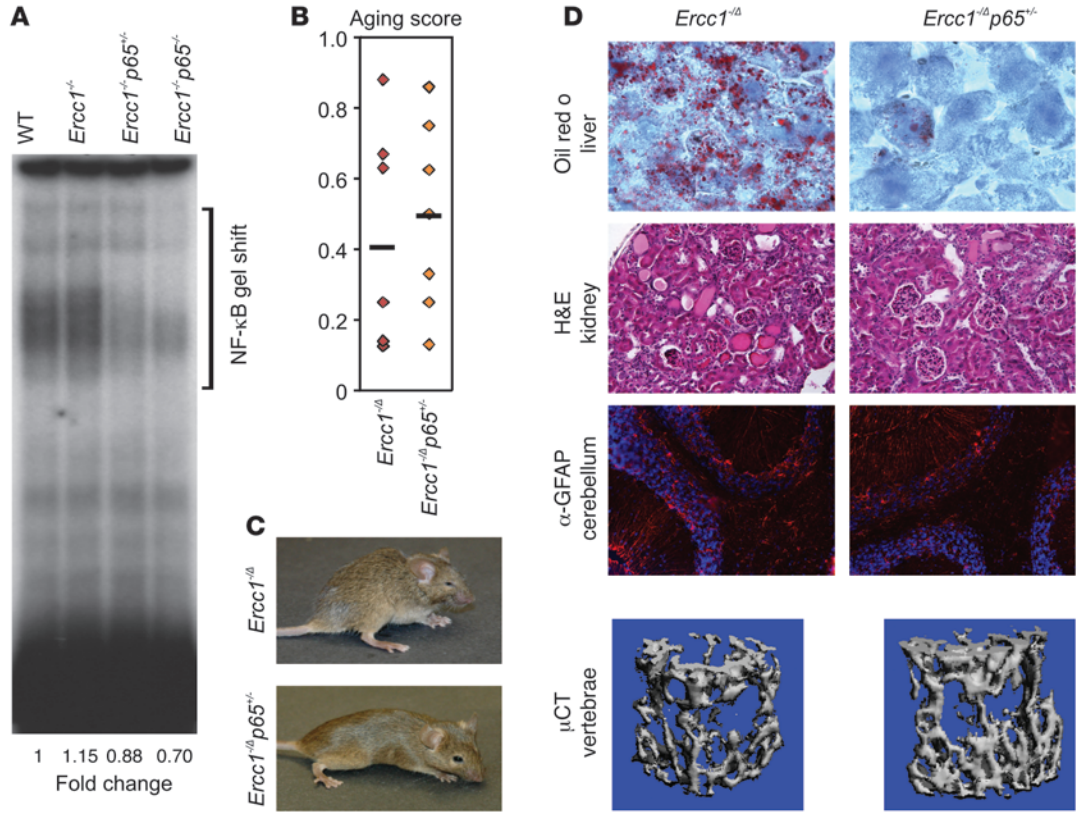

Figure 2

Genetic depletion of the p65 subunit of NF-κB delays aging symptoms and chronic diseases in progeroid *Ercc1*$^{-/\Delta}$ mice. (**A**) EMSA on nuclear extracts from passage 5 WT, *Ercc1*$^{-/-}$, *Ercc1*$^{-/-}$*p65*$^{+/-}$, and *Ercc1*$^{-/-}$*p65*$^{-/-}$ MEFs grown at 20% O_2 to measure NF-κB activity after depletion of p65. (**B**) *Ercc1*$^{-/\Delta}$ and *Ercc1*$^{-/\Delta}$*p65*$^{+/-}$ mice were evaluated biweekly for the onset of spontaneous symptoms associated with aging. The aging score, which represents the fraction of aging symptoms delayed in a particular mouse compared with its sibling, for littermate pairs of *Ercc1*$^{-/\Delta}$ (red) and *Ercc1*$^{-/\Delta}$*p65*$^{+/-}$ (orange) mice is a measure of healthspan (11). The mean aging score for each genotype is represented by a black bar. (**C**) Representative images of *Ercc1*$^{-/\Delta}$ and *Ercc1*$^{-/\Delta}$*p65*$^{+/-}$ sex-matched littermates at 15 weeks of age. (**D**) Histopathologic changes in *Ercc1*$^{-/\Delta}$*p65*$^{+/-}$ and *Ercc1*$^{-/\Delta}$ mice. Liver sections from 10-week-old mice were stained with oil red O to detect neutral lipids (hepatic steatosis; original magnification, ×100). Kidney specimens from 15-week-old mice were stained with H&E to detect proteinaceous renal tubular hyaline casts and glomerulosclerosis (original magnification, ×20). Cerebellar sections from 10-week-old mice were immunostained for GFAP (red), a marker of neurodegeneration. Nuclei were counterstained with DAPI (blue; original magnification, ×40). μCT of the vertebrae to assess bone porosity (for quantification, see Supplemental Figure 3A).

whether NF-κB is also upregulated in the progeroid mouse model, kidney specimens from *Ercc1*$^{-/\Delta}$NF-κB^{EGFP} mice (life span, 7 months; ref. 49) and WT NF-κB^{EGFP} littermates were isolated at 3 months of age (Figure 1B) and kidney specimens from *Ercc1*$^{-/-}$NF-κB^{EGFP} mice (life span, 28 days; ref. 45) and WT NF-κB^{EGFP} littermates were isolated at 21 days of age (Figure 1C) to measure EGFP expression. Similar to natural aging, NF-κB activity was greater in the kidneys of ERCC1-deficient mice, particularly in the glomeruli, compared with that in WT littermates. In addition, EGFP$^+$ cells were detected in the livers, pancreata, spleens, and muscle of *Ercc1*$^{-/-}$NF-κB^{EGFP} mice (Supplemental Figure 1; supplemental material available online with this article; doi:10.1172/JCI45785DS1). Among 6 littermate pairs, we detected a significant increase in the fraction of EGFP$^+$ cells in the progeroid mice relative to that in WT littermates: kidney (2.5-fold increase), pancreas (2.5-fold increase), muscle (1.7-fold increase), and liver (4-fold increase) (Figure 1D). In contrast, the percentage of EGFP$^+$ cells was 35% lower in the spleens of *Ercc1*$^{-/-}$NF-κB^{EGFP} mice than in those of WT NF-κB^{EGFP} littermates, indicating that NF-κB activation is not exclusively driven by inflammation. These data support earlier reports (22, 23) that there is increased NF-κB activation with mammalian aging and extend this to include a murine model of XFE progeroid syndrome, which is driven by a DNA repair defect.

To confirm that NF-κB activity is increased in cells from progeroid *Ercc1*$^{-/-}$ mice, the levels of phosphorylated p65 (p-p65) and IκB were measured by immunoblot in nuclear and cytoplasmic extracts from passage 5, congenic *Ercc1*$^{-/-}$ and WT primary mouse embryonic fibroblasts (MEFs). There was a more than 2-fold increase in nuclear p-p65 in *Ercc1*$^{-/-}$ MEFs compared with that in WT MEFs (Figure 1E), which correlated with an increase in the level of phosphorylated IκB (p-IκB) in the cytoplasm. Increased NF-κB binding activity was also detected in nuclear extracts from *Ercc1*$^{-/-}$ MEFs by EMSA (Figure 1F). Pretreatment of the nuclear lysates with anti-p50 and, in particular, anti-p65 antibodies reduced this DNA binding activity (Supplemental Figure 2). These data establish increased NF-κB activity in DNA repair–deficient *Ercc1*$^{-/-}$ cells from progeroid mice and suggest that p65 is the predominant subunit contributing to this increased activity.

Table 1
Genetic depletion of the p65 subunit of NF-κB delays aging symptoms of progeroid *Ercc1*$^{-/\Delta}$ mice

Symptoms	Age at onset (wk)		Change of onset (wk)	No. of *Ercc1*$^{-/\Delta}$ mice (WT, *p65*$^{+/-}$)
	Ercc1$^{-/\Delta}$	*Ercc1*$^{-/\Delta}$*p65*$^{+/-}$		
Dystonia	7.3	7.0	–0.3	7, 7
Trembling	7.0	7.1	**0.1**	7, 7
Kyphosis	9.8	11.1	**1.3**	7, 7
Ataxia	12.1	11.3	–0.8	7, 7
Sarcopenia	13.3	13.8	**0.5**	7, 7
Spontaneous activity	19.4	17.2	–2.2	5, 5
Urinary incontinence	15.9	19.3	**3.4**	4, 2

Ercc1$^{-/\Delta}$ and *Ercc1*$^{-/\Delta}$*p65*$^{+/-}$ mice were evaluated biweekly for the onset of spontaneous symptoms associated with aging. The average age at onset of each symptom for each group and the difference between the group averages is shown. Symptoms delayed in the *p65* heterozygous mice are indicated in bold.

Genetic reduction of NF-κB delays the onset of progeroid symptoms in Ercc1$^{-/\Delta}$ *mice*. To determine whether NF-κB activation drives age-related pathologies, *Ercc1*$^{-/\Delta}$ mice were bred to have a deletion of one allele of the NF-κB subunit, p65 (*Ercc1*$^{-/\Delta}$*p65*$^{+/-}$ mice). To determine whether genetic depletion of p65 indeed resulted in reduced NF-κB DNA binding activity, EMSAs were performed using extracts from WT, *Ercc1*$^{-/-}$, *Ercc1*$^{-/-}$*p65*$^{+/-}$, and *Ercc1*$^{-/-}$*p65*$^{-/-}$ primary MEFs (Figure 2A). Heterozygosity of p65 resulted in a reduction in NF-κB binding activity, whereas homozygous deletion of p65 reduced NF-κB binding activity even further.

To examine the role of NF-κB/p65 in the aging process, *Ercc1*$^{-/\Delta}$ and *Ercc1*$^{-/\Delta}$*p65*$^{+/-}$ littermates were monitored biweekly for the onset of age-related symptoms. The onset of the majority of symptoms characteristic of *Ercc1*$^{-/\Delta}$ mice was delayed in *Ercc1*$^{-/\Delta}$*p65*$^{+/-}$ mice, including trembling, kyphosis, sarcopenia, and urinary incontinence — all signs of neurodegeneration (Table 1). The aging score, representing the fraction of all aging-related symptoms that were delayed in *Ercc1*$^{-/\Delta}$*p65*$^{+/-}$ mice compared with that in littermate *Ercc1*$^{-/\Delta}$ mice, revealed a trend toward a delay in onset of aging pathologies (Figure 2B). Additionally, the overall physical appearance of the *Ercc1*$^{-/\Delta}$*p65*$^{+/-}$ mice was dramatically improved (Figure 2C). At 15 weeks of age, *Ercc1*$^{-/\Delta}$ mice exhibited ocular impairment, a wide-base stance (ataxia), sarcopenia, kyphosis, and frailty — all of which were dramatically attenuated in *Ercc1*$^{-/\Delta}$*p65*$^{+/-}$ mice.

In addition to assessing outward signs of aging, histologic analysis was performed. Mice were euthanized at 10 and 15 weeks of age, and tissues were collected for analysis of several hallmarks of age-related degeneration. Compared with *Ercc1*$^{-/\Delta}$ mice, *Ercc1*$^{-/\Delta}$*p65*$^{+/-}$ mice exhibited a marked reduction of steatosis (Figure 2D), a marker of aged liver (50). Kidneys from *Ercc1*$^{-/\Delta}$ mice had increased proteinaceous renal tubular hyaline casts and glomerulosclerosis (Figure 2D), typical of aged kidneys (51, 52), that was reduced in *Ercc1*$^{-/\Delta}$*p65*$^{+/-}$ mice. There also was a reduction in glial fibrillary acidic protein (GFAP) staining, a marker of neurodegeneration (53), in the cerebella of *Ercc1*$^{-/\Delta}$*p65*$^{+/-}$ mice compared with that in *Ercc1*$^{-/\Delta}$ littermates (Figure 2D). Finally, osteoporosis was significantly reduced in *Ercc1*$^{-/\Delta}$*p65*$^{+/-}$ mice (Figure 2D and Supplemental Figure 3A). Taken together, these results demonstrate that reducing NF-κB activity delays the onset of numerous age-related pathologies and extends healthspan.

Pharmacologic inhibition of NF-κB delays the onset of progeroid symptoms in Ercc1$^{-/\Delta}$ *mice*. To determine whether pharmacologic suppression of IKK/NF-κB signaling also results in an extension of healthspan, a peptide inhibitor of IKK, termed the NEMO-binding domain (NBD), was used. The 11–amino acid NBD peptide, when fused to a protein transduction domain such as Antp or 8K, is efficacious for treating muscular dystrophy (54), inflammatory bowel disease (55), arthritis (56), and Parkinson's disease (57) in mice. The activity of the peptide was tested in vitro by treating *Ercc1*$^{-/-}$ primary MEFs with 200 μM 8K-NBD. This led to a reduction in nuclear p-p65 (Figure 3A). *Ercc1*$^{-/\Delta}$ mice were chronically treated with 8K-NBD (10 mg/kg i.p., 3 times per week) beginning at 5 weeks of age, which is prior to the onset of their aging symptoms. Littermate mutant animals were treated with an equivalent dose of an inactive, mutant peptide (8K-mNBD) used as a negative control. Investigators conducting the experiment were blinded to the treatment group. Mice treated with 8K-NBD showed a delay in the onset of the majority of symptoms compared with siblings treated with the mutant peptide (Table 2). Ataxia, sarcopenia, and weight loss were significantly delayed (Table 2 and Supplemental Figure 4B). In addition, the aging score revealed a highly significant difference between treatment groups ($P = 0.003$; Figure 3B). There also was a visible difference in the appearance of the mice treated with 8K-NBD compared with that of their siblings treated with the mutant peptide at 15 and 19 weeks of age (Figure 3C) as well as improved reflexes, gait, muscle, and eyes.

Histologic analysis was performed on tissues of 19-week-old mice to determine whether treatment with 8K-NBD reduced age-related pathology. Similar to that in the *Ercc1*$^{-/\Delta}$*p65*$^{+/-}$ mice, 8K-NBD treatment resulted in reduced liver steatosis and renal hyaline casts compared with that in control mice (Figure 3D). GFAP staining was also reduced, consistent with the delay in onset of symptoms caused by neurodegeneration (Figure 3D). Microcomputed tomography (μCT) analysis revealed a significant reduction in bone porosity (osteoporosis) in mice treated with 8K-NBD compared with that in untreated *Ercc1*$^{-/\Delta}$ mice (Figure 3D and Supplemental Figure 3B). Collectively these data demonstrate that pharmacological inhibition of IKK/NF-κB activation leads to attenuation of age-related pathologies.

Unexpectedly, the age at onset of progeroid symptoms was delayed slightly in mutant animals treated with the mutant NBD peptide compared with that in untreated mutant animals (compare Table 2 with Table 1), suggesting that the mutant peptide has residual activity, which was confirmed in cell culture assays (data not shown). Therefore, we also compared the age at onset of symptoms in *Ercc1*$^{-/\Delta}$ mice treated with 8K-NBD with that of *Ercc1*$^{-/\Delta}$ mice treated with vehicle only (PBS) (Supplemental Table 1). This comparison revealed a significant delay in the onset of even more symptoms in mice treated with 8K-NBD (trembling, ataxia, sarcopenia) and a more significant delay of all symptoms assessed. At 15 weeks of age, *Ercc1*$^{-/\Delta}$ mice exhibited dystonia and cachexia, and, by 19 weeks of age, incontinence, ocular defects, and sarcopenia were obvious (Supplemental Figure 5). *Ercc1*$^{-/\Delta}$

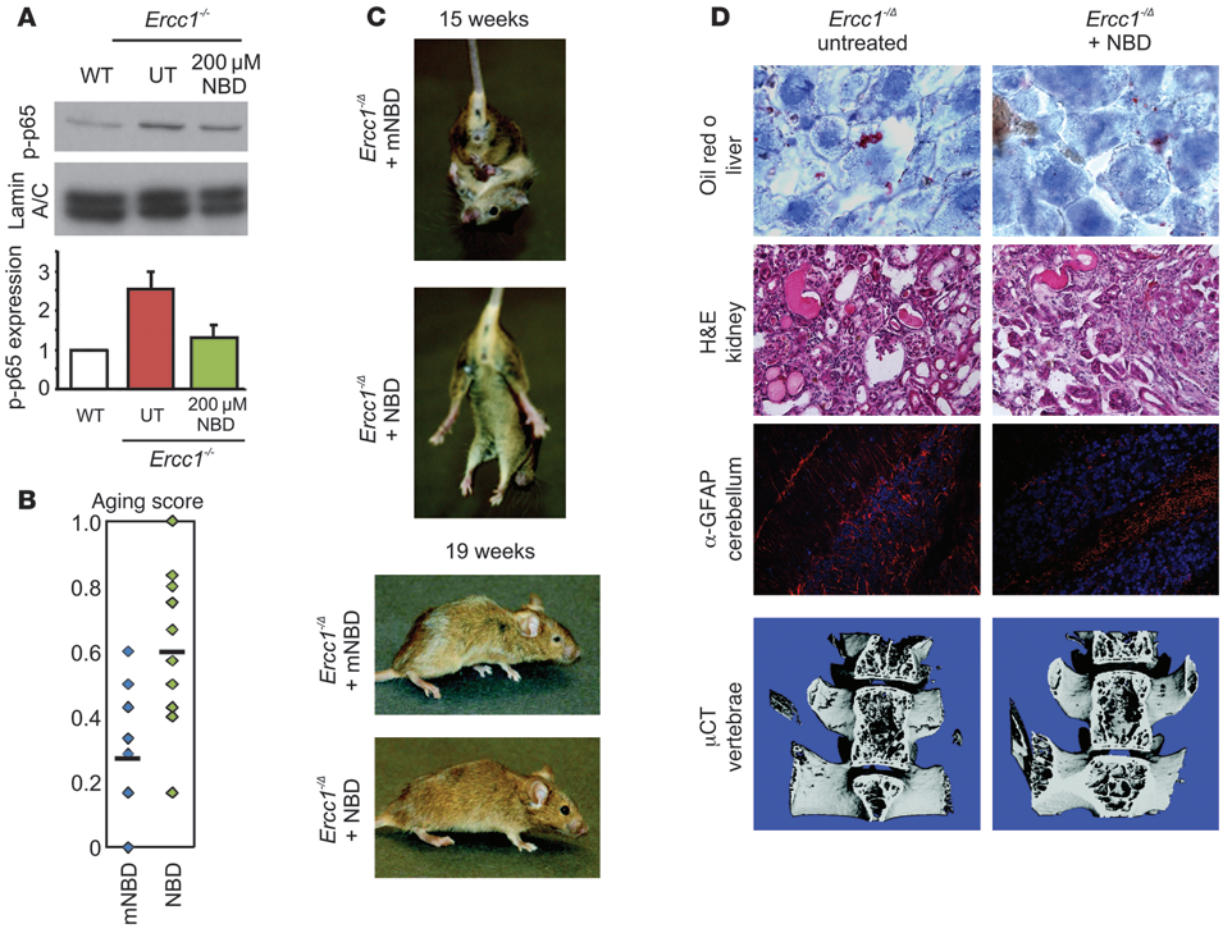

Figure 3

Pharmacologic inhibition of IKK/NF-κB activation delays aging symptoms and chronic diseases in progeroid *Ercc1*$^{-/\Delta}$ mice. (**A**) Immunodetection of p-p65 in nuclear extracts of WT or *Ercc1*$^{-/-}$ primary MEFs treated with 200 μM NBD or untreated (UT). Lamin A/C was used as a loading control. The histogram indicates the level of p-p65 normalized to that of untreated WT cells and corrected for loading. Values denote mean ± SD from 3 experiments. (**B**) Sibling, sex-matched pairs of *Ercc1*$^{-/\Delta}$ mice were treated with 10 mg/kg 8K-NBD or 8K-mNBD i.p., 3 times per week, beginning at 5 weeks of age. The aging score was calculated between *Ercc1*$^{-/\Delta}$ littermate pairs treated with 8K-mNBD (blue) or 8K-NBD (green). The mean aging score is represented by a black bar ($P = 0.003$, Student's *t* test). (**C**) Representative images of *Ercc1*$^{-/\Delta}$ mice treated with 8K-NBD or 8K-mNBD peptide at 15 and 19 weeks of age. (**D**) Histopathologic changes analyzed in tissue sections from 18-week-old *Ercc1*$^{-/\Delta}$ mice treated with 8K-NBD or untreated. Liver sections were stained with oil red O to detect neutral lipids (hepatic steatosis; original magnification, ×100). Kidney specimens were stained with H&E to detect hyaline casts and glomerulosclerosis (original magnification, ×20). Cerebellar sections were immunostained for GFAP (red), a marker of neurodegeneration. Nuclei were counterstained with DAPI (blue; original magnification, ×40). μCT of vertebrae to measure bone porosity (for quantification, see Supplemental Figure 3B).

mice treated with 8K-NBD were largely spared these symptoms. These data demonstrate that pharmacologic inhibition of NF-κB activation can be used to simultaneously delay the onset of symptoms associated with multiple, common, age-related chronic degenerative diseases.

8K-NBD alters NF-κB signaling in vivo. To determine whether 8K-NBD indeed affects NF-κB–regulated gene expression in vivo, the gene expression profile of livers of 19-week-old *Ercc1*$^{-/\Delta}$ mice chronically exposed to 8K-NBD was compared with that of littermate mutant animals treated with 8K-mNBD. A full mouse genome array revealed 1,269 genes (~5% of all genes) with significantly changed expression patterns when comparing 8K-NBD–treated and 8K-mNBD–treated mice ($P \leq 0.05$, 1.2-fold change upregulated or downregulated). Of the 29 genes with known NF-κB regulatory elements that significantly differed between treatment groups, 26 were significantly downregulated in mice treated with 8K-NBD (Table 3), demonstrating that 8K-NBD treatment reduces NF-κB activity in vivo.

All genes with significantly altered expression were grouped according to their known or predicted biological function into gene ontology (GO) categories. Significantly altered biological processes were identified as those with a disproportionate number of genes having altered expression relative to those printed on the Affymetrix chip. Five major biological processes were significantly suppressed in response to inhibition of NF-κB. These processes, ranked by their relative enrichment score, included immune responses, cell cycle regulation, apoptosis, stress and DNA damage responses, and growth hormone signaling (Figure 4A). Of note, NF-κB is known to regulate many of these processes, and NF-κB activation was one of the GO categories identified as suppressed in

Table 2
Pharmacologic suppression of IKK/NF-κB activation attenuates progeroid symptoms and pathologies of progeroid *Ercc1*$^{-/\Delta}$ mice

Symptoms	Age at onset (wk)		Change of	No. of *Ercc1*$^{-/\Delta}$
	mNBD	NBD	onset (wk)	mice (mNBD, NBD)
Dystonia	9.2	9.1	–0.1	12, 17
Trembling	10.7	9.8	–0.9	12, 17
Kyphosis	12.9	12.2	–0.7	11, 15
Ataxia[A]	14.5	16.2	**1.7**	10, 13
Sarcopenia[A]	15.1	17.2	**2.1**	8, 12
Spontaneous activity	20.4	10.7	**0.3**	3, 2
Urinary incontinence	17.5	19.7	**2.2**	5, 3

Sibling, sex-matched pairs of *Ercc1*$^{-/\Delta}$ mice were treated with 10 mg/kg 8K-NBD or 8K-mNBD i.p., 3 times per week, beginning at 5 weeks of age and continuing throughout their life span. The average age at onset of characteristic progeroid symptoms in treated *Ercc1*$^{-/\Delta}$ mice and the difference between the group averages is shown. Symptoms delayed in mice treated with the NF-κB inhibitor 8K-NBD compared with those in mice treated with 8K-mNBD are indicated in bold. [A]Significant delay ($P < 0.05$; Student's *t* test).

tissues from mice chronically treated with 8K-NBD (Figure 4A). To validate the microarray data, the expression of a number of NF-κB target genes, including *Apod*, *Gadd45b*, *Bcl2*, *Lamb2*, *Icam1*, *Plcd1*, and *Sod1*, was measured using qRT-PCR (Figure 4B). Expression of the majority of these genes was confirmed to be reduced in mice treated with 8K-NBD relative to that in littermates treated with the control peptide ($n = 4$ mice per group; Figure 4B).

The expression of key genes known to be altered in old WT mice was also evaluated by qRT-PCR (47). The growth hormone/IGF-1 axis is downregulated in aged mice and progeroid ERCC1-deficient mice (45). Interestingly, chronic treatment with 8K-NBD led to an increase in expression of many of these genes involved in these pathways, including *Ghr*, *Prlr*, and *Dio2* (Figure 4B).

Inhibition of NF-κB reduces senescence in vitro and in vivo. To examine the mechanism through which NF-κB inhibition extends healthspan, we examined the role of NF-κB in regulating cellular senescence in vitro. Primary MEFs grown in atmospheric oxygen senesce prematurely due to oxidative stress (58). DNA repair–deficient *Ercc1*$^{-/-}$ MEFs senesce even earlier than congenic WT cells (Figure 5A). This corresponded with increased γH2AX foci (Figure 5B), a marker of cellular senescence (59). Deletion (*Ercc1*$^{-/-}$*p65*$^{-/-}$ MEFs) or p65 heterozygosity (*Ercc1*$^{-/-}$*p65*$^{+/-}$ MEFs) rescued proliferation and senescence to a large extent (Figure 5, A and B). Hepatocytes of *Ercc1*$^{-/\Delta}$ mice show profound cellular senescence (44). Reduced expression of p65 resulted in a significant reduction in the number of senescent hepatocytes in *Ercc1*$^{-/\Delta}$ mice (Figure 5C). In addition, p16^{INK4a} expression was dramatically reduced in the livers of *Ercc1*$^{-/\Delta}$ mice chronically treated with 8K-NBD compared with that in untreated animals (Figure 5D), consistent with the qRT-PCR results (Figure 4B). Taken together, these results demonstrate that reducing NF-κB/p65 activity attenuates cellular senescence, at least under conditions of stress.

Inhibition of NF-κB reduces oxidative stress and damage in vitro and in vivo. A key driver of cellular senescence is genotoxic stress (60). Hence, we next asked whether NF-κB activation in ERCC1-deficient cells regulates oxidative stress. *Ercc1*$^{-/-}$ and *Ercc1*$^{-/-}$*p65*$^{-/-}$ primary MEFs grown at 20% O_2 were stained with $DiOC_6$ to identify mitochondria and with MitoSOX to measure superoxide anion in mitochondria. *Ercc1*$^{-/-}$*p65*$^{-/-}$ MEFs had reduced mitochondrial ROS compared with that of *Ercc1*$^{-/-}$ MEFs (Figure 6A). This was supported by the observation that *Ercc1*$^{-/\Delta}$*p65*$^{+/-}$ mice have less lipofuscin in their livers than *Ercc1*$^{-/\Delta}$ mice (Figure 6B). Lipofuscin is an accumulation of oxidized fatty acids associated with aging (61–64). We also examined the levels of a unique type of oxidatively induced DNA lesions, 8,5′-cyclopurine-2′-deoxynucleosides (cPu), which include 8,5′-cyclo-2′-deoxyadenosine (cdA) and 8,5′-cyclo-2′-deoxyguanosine (cdG). These lesions may serve as reliable biomarkers of oxidative DNA damage, because they are rather stable and O_2 inhibits their formation, thus minimizing their artificial generation during DNA extraction and enzymatic digestion (65). Levels of all 4 cPu lesions, i.e., *R*- and *S*-diastereomers of cdG and cdA, were significantly decreased in *Ercc1*$^{-/\Delta}$*p65*$^{+/-}$ mice compared with those in *Ercc1*$^{-/\Delta}$ littermates (Figure 6C). This was also true in *Ercc1*$^{-/\Delta}$ mice chronically treated with 8K-NBD compared with untreated mutant animals (Figure 6D). Genetic depletion of p65 also reduced the amount of oxidative DNA damage in WT mice (Figure 6C; compare controls with *p65*$^{+/-}$ mice). These data provide multiple lines of evidence supporting the conclusion that reduction in NF-κB activity leads to an attenuation of oxidative stress and damage.

Discussion

Time-dependent accumulation of damage to cells and macromolecules is thought to drive aging (2). DNA damage is one type of damage implicated in aging based on the fact that mutations affecting a diverse array of DNA repair mechanisms lead to accelerated aging of one or more tissues (66). However, what is not known is the mechanism by which, for instance, damage to the nuclear genome drives aging. The mechanism could be via loss of functional cells once a threshold of damage is reached. Alternatively, activation of conserved stress response pathways may promote aging. Herein, to decipher how damage drives aging, we used a well-defined murine system: mice that spontaneously age rapidly as a consequence of failure to repair endogenous DNA damage (44, 49, 67).

The NF-κB family consists of transcription factors activated in response to a diverse array of cellular stressors (68). NF-κB activity increases with chronologic age in a variety of tissues of mammals (24–28). Thus, NF-κB activation could drive aging in response to time-dependent accumulation of cell damage. However, prior studies do not demonstrate a causal relationship between NF-κB activation and aging; neither do they reveal what drives NF-κB activation with aging.

Using a knockin NF-κB^{EGFP} reporter system, we discovered a significant increase in the percentage of cells in which NF-κB was activated in old and DNA repair–deficient, progeroid mice relative to that in young WT mice. The progeroid mice had increased EGFP expression in kidneys, skeletal muscle, pancreata, and livers (Figure 1 and Supplemental Figure 1). There was not significantly greater NF-κB activation in the spleen, suggesting that inflammatory cells are not the primary driver of NF-κB activation. These data strongly support the conclusion that spontaneous, endogenous DNA damage is sufficient to drive NF-κB activation in vivo. The resolution afforded by the reporter construct revealed that age-related activation of NF-κB is stochastic, meaning that there is activation in one cell while none is detected in adjacent cells,

Table 3
8K-NBD inhibits NF-κB in vivo and corrects gene expression changes associated with aging

Gene symbol	Fold change	*P* value
Csf3	1.8	0.001
Agt	1.2	0.02
Sod1	1.1	0.04
Ctsb	–1.1	0.02
Eng	–1.2	0.05
Il15ra[A]	–1.2	0.001
Scarb1	–1.2	0.02
Prkcd[B]	–1.2	0.01
Icam1[A]	–1.3	0.01
Nfkbia	–1.3	0.02
Ccnd3[B]	–1.3	0.03
Ccl19[A]	–1.4	0.04
Tcrg[A]	–1.4	0.01
App	–1.5	0.03
Bcl2[B]	–1.5	0.007
Plcd1	–1.6	0.03
Ccnd2[B]	–1.7	0.02
Cd48[A]	–1.7	0.03
Sdc4	1.5	0.006
Abcb1a	–1.8	0.04
Cd80[A]	–1.9	0.03
Upk1b	–1.9	0.03
Oas3	–2.0	0.03
Penk[B]	–2.1	0.009
Ighg1[A]	–2.4	0.03
Ptx3[A]	–2.4	0.01
Lamb2[B]	–2.5	0.009
Gadd45b[B]	–3.5	0.02
Apod[B]	–4.4	0.01

RNA was isolated from the livers of 18- to 19-week-old *Ercc1*$^{-/\Delta}$ mice chronically treated with 8K-NBD or 8K-mNBD (n = 4 per group). Differences in gene expression were analyzed using total genome Affymetrix arrays. Genes with known NF-κB regulatory elements that were significantly altered in *Ercc1*$^{-/\Delta}$ mice treated with 8K-NBD compared with those in mice treated with 8K-mNBD are shown. [A]Genes implicated in inflammation. [B]Genes implicated in cell survival and cell cycle control.

rather than pan-activation throughout a tissue. This is consistent with the stochastic theory of aging, which posits that cellular damage occurs randomly in a fraction of cells (2).

We also demonstrate a key causal role for NF-κB in driving multiple age-related pathologies. Inhibition of the IKK/NF-κB pathway genetically, through deletion of one copy of *p65*, or pharmacologically, using an IKK inhibitory peptide, delayed the onset and severity of aging-related pathologies in the musculoskeletal, hepatobiliary, renal, and nervous systems (Figure 2D and Figure 3D). Aging-related symptoms caused by these pathologies were also delayed or attenuated (Tables 1 and 2). This provides strong experimental evidence that an increase of IKK/NF-κB activity plays a causal role in aging.

We further demonstrate that genetic reduction of NF-κB reduced the amount of mitochondrial-derived ROS (Figure 6A). This could be mediated through upregulation of antioxidants. Expression of catalase and targets of NRF2 was significantly increased in mice chronically treated with the IKK inhibitor 8K-NBD (Figure 4) compared with that in mice treated with an inactive mutant peptide. In further support of this, oxidative damage to lipids (lipofuscin; Figure 6B) and DNA (Figure 6, C and D) was significantly reduced in *Ercc1*$^{-/-}$*p65*$^{+/-}$ mice and *Ercc1*$^{-/-}$ mice chronically treated with the IKK inhibitor 8K-NBD. This corresponded with a reduction in multiple markers of cellular senescence, including reduced proliferation of primary cells, increased γH2AX foci, and senescence-associated β-galactosidase (SA β-gal) activity. These data support a mechanism by which accumulated cellular damage (in particular DNA damage) with aging leads to activation of NF-κB. This in turn drives increased ROS production and even more cellular damage. Inhibiting NF-κB activation in response to stress is sufficient to attenuate damage and extend healthspan of a murine model of accelerated aging.

Interestingly, our data indicate that treating *Ercc1*$^{-/\Delta}$ mice with 8K-NBD, beginning at 5 weeks of age, has a greater beneficial effect than genetic depletion of p65 from conception. The delay in aging symptoms, the attenuation of osteoporosis, and the maintenance of weight (Supplemental Figure 4) were greater in mice in which NF-κB activity was inhibited pharmacologically compared with those with genetic inhibition. This could be because p65/NF-κB has a positive role during development and/or early in life. Also, *p65* was heterozygous in our mice, and therefore it is possible that the remaining copy of *p65* is sufficient to initiate a stress response. Alternatively, 8K-NBD may be more effective at inhibiting NF-κB in response to stress, possibly because inhibition of IKK would act upstream of p65 and could lead to the cytoplasmic sequestration of more than just the p65 subunit of NF-κB. Targeting IKK also may affect other pathways in addition to NF-κB. For example, IKK phosphorylates BCL-10, β-catenin, cyclin D1, FOXO3A, p53, ERα, mTOR, and HIF-1α in addition to NF-κB (69–72).

The magnitude of the effect on healthspan elicited by NF-κB inhibition has only been observed in outbred mice treated with rapamycin (73), which targets the mTOR pathway, or by genetic deletion of S6K1, a downstream target of mTOR (74). Interestingly, mTOR has been shown to activate NF-κB via interaction with IKK (75). In contrast to the results with rapamycin and our results with NBD, treatment with resveratrol and other SIRT agonists appears only able to extend healthspan and life span in mice on high-fat diets (76).

Interestingly, chronic inhibition of NF-κB with the 8K-NBD peptide caused a dramatic change in gene expression compared with that in *Ercc1*$^{-/\Delta}$ littermates treated with a less active control peptide. Expression of 5% of all genes was significantly altered. Based on ontology analysis of these genes, the biological process most significantly affected by NF-κB inhibition was the immune response, which was not surprisingly downregulated. In addition, many processes previously demonstrated to be altered in progeroid or old WT mice, including suppression of the growth hormone/IGF-1 axis, inhibition of cell cycle progression, activation of proapoptotic mechanisms, and DNA damage/stress response (45), were at least partially corrected by NF-κB inhibition. This provides experimental evidence that NF-κB is indeed a master regulator of aging-related transcriptional reprogramming.

Gene expression analysis also confirmed the efficacy of inhibition of IKK/NF-κB by 8K-NBD, demonstrating decreased expression of numerous genes with known NF-κB promoter sequences, including *Gadd45b*, *Ccnd2*, *Ccnd3*, *Bcl2*, *Apod*, and *Prkcd* (77). The NF-κB–regulated genes that were most downregulated by 8K-NBD were *Apod* and *Gadd45*, both of which have been shown to have roles in cellular senescence and age-related disease (78, 79). Similarly, a number of cytokines and other proinflammatory genes expressed by senescent cells (80) are downregulated

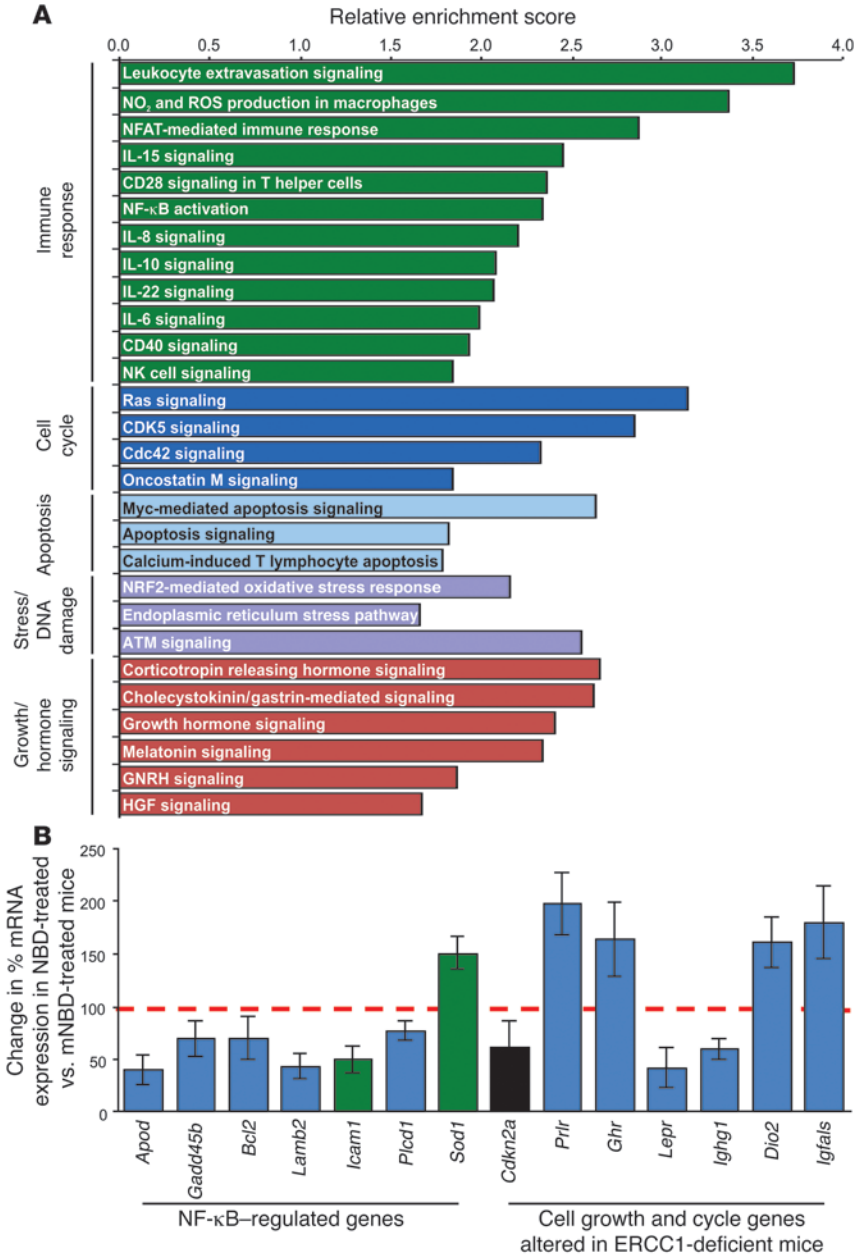

Figure 4

8K-NBD inhibits NF-κB in vivo and corrects gene expression changes associated with aging. RNA was isolated from livers of 18- to 19-week-old *Ercc1*$^{-/\Delta}$ mice chronically treated with 8K-NBD or 8K-mNBD (n = 4 per group). Differences in gene expression were analyzed using total genome Affymetrix arrays. (**A**) GO enrichment analysis of the networks and pathways regulated by 8K-NBD. The biological processes most significantly affected by chronic inhibition of IKK/NF-κB are ranked by their relative enrichment score. GNRH, gonadotropin-releasing hormone. (**B**) qRT-PCR of genes identified by microarray analysis to be significantly differentially expressed in *Ercc1*$^{-/\Delta}$ mice chronically treated with 8K-NBD relative to sibling mutant animals treated with 8K-mNBD. The dashed red line indicates mean expression in mice treated with the mutant peptide. The bars indicate the mean expression in mice treated with the NF-κB inhibitor 8K-NBD (n = 4 per treatment group) ± SD. For the NF-κB–regulated genes, green coloring indicates genes implicated in inflammation. Blue coloring indicates genes implicated in cell survival. Expression of *Cdkn2a* (the gene encoding p16^{INK4a}), a marker of cellular senescence, is in black.

in *Ercc1*$^{-/\Delta}$ mice chronically treated with 8K-NBD, notably *Il16*, *Il17ra*, *Il20*, *Il1r1*, *Il15ra*, *Il28ra*, *Ildr1*, and *Il6st*. 8K-NBD treatment also reduced liver expression of p16 at both the mRNA and protein level. Moreover, chronic 8K-NBD treatment significantly upregulated catalase, genes regulated by NRF2, and genes involved in mitochondrial respiration, all important in regulating ROS levels. These observations are consistent with the recent demonstration of a key role for p16-expressing senescent cells in driving aging, suggesting that 8K-NBD treatment can reduce senescence (81). 8K-NBD treatment also suppressed expression of chemokines known to regulate the trafficking of immune cells during inflammation. Overall, the expression data demonstrate that inhibition of IKK/NF-κB leads to suppression of numerous processes that are known to modulate healthspan, including inflammation and cellular senescence.

In conclusion, these studies demonstrate that spontaneous, endogenous DNA damage can activate NF-κB. Activation of NF-κB is stochastic, occurring only in a subset of cells. Chronic inhibition of IKK/NF-κB activation is sufficient to delay the onset of aging symptoms and chronic aging-related diseases that arise spontaneously in DNA repair–deficient *Ercc1*$^{-/\Delta}$ mice that model a human progeroid syndrome. Moreover, inhibiting NF-κB activation reduces ROS production and oxidative damage to lipids and DNA. This demonstrates a direct causal role for NF-κB in driving aging-related changes in response to cellular damage by promoting continued damage. Inhibition of NF-κB offers what we believe to be a novel strategy for simultaneously delaying and/or attenuating multiple chronic degenerative diseases in patients with progeroid syndromes and potentially in old age.

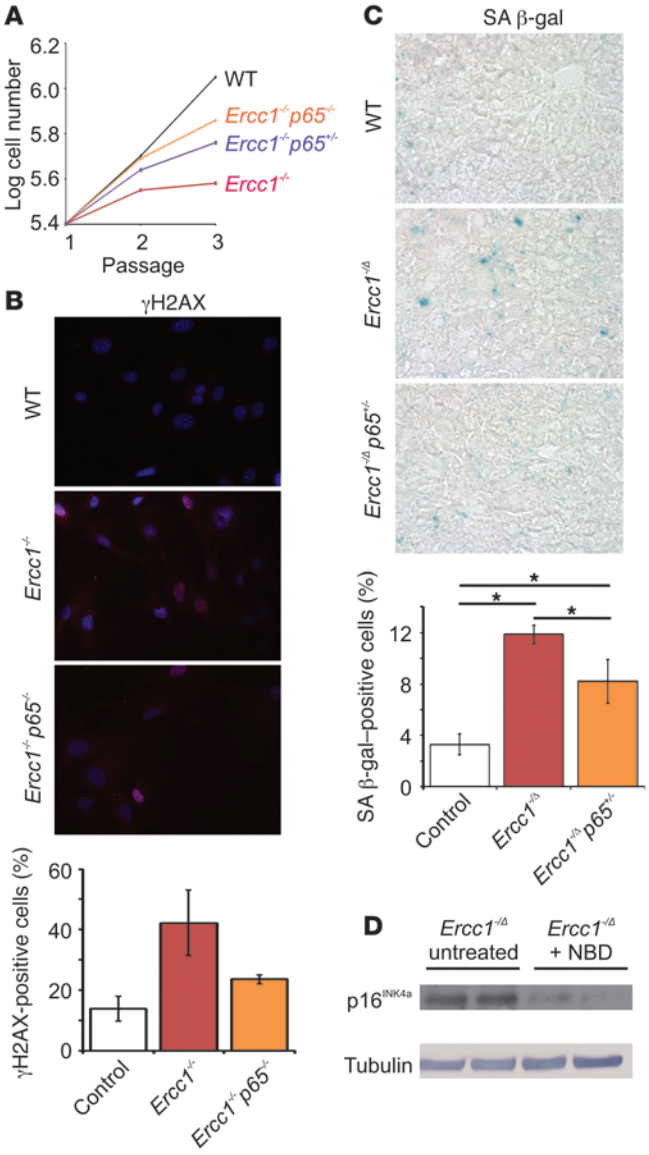

Figure 5
Inhibition of NF-κB reduces cellular senescence in vitro and in vivo. (**A**) Proliferation of WT (black; $n = 4$), *Ercc1*$^{-/-}$ (red; $n = 3$), *Ercc1*$^{-/-}$*p65*$^{+/-}$ (purple; $n = 1$) and *Ercc1*$^{-/-}$*p65*$^{-/-}$ (orange; $n = 3$) congenic primary MEFs grown at 20% O_2 for several passages. *Ercc1*$^{-/-}$ MEFs grew slower than WT MEFs, while *Ercc1*$^{-/-}$*p65*$^{-/-}$ MEFs showed better growth compared with that of *Ercc1*$^{-/-}$ MEFs. (**B**) γH2AX staining (red) of passage 5 WT, *Ercc1*$^{-/-}$, and *Ercc1*$^{-/-}$*p65*$^{-/-}$ primary MEFs grown at 20% O_2. Nuclei were counterstained with DAPI (blue; original magnification, ×20). The histogram indicates the percentage of cells positive for γH2AX foci. (**C**) SA β-gal staining of liver sections from 10-week-old control, *Ercc1*$^{-/\Delta}$, and *Ercc1*$^{-/\Delta}$*p65*$^{+/-}$ mice (original magnification, ×40). The histogram indicates the percentage of SA β-gal–positive cells from 5 images from at least 9 mice per genotype. Values denote the mean ± SEM. $^*P < 0.05$, Tukey-Kramer test. (**D**) Immunodetection of p16 in liver extracts of 19-week-old untreated *Ercc1*$^{-/\Delta}$ and NBD-treated *Ercc1*$^{-/\Delta}$ mice.

Methods

Mice. *Ercc1*$^{-/-}$ and *Ercc1*$^{-/\Delta}$ mice were generated in an F_1 hybrid background by crossing heterozygous *Ercc1*$^{+/-}$ and *Ercc1*$^{+/\Delta}$ mice from 2 different inbred C57BL/6J and FVB/n backgrounds to obtain genetically identical mice, without strain-specific pathology. The mice were genotyped using PCR as previously described (82). *Ercc1*$^{-/-}$NF-κB^{EGFP} mice were generated by crossing *Ercc1*$^{+/-}$ C57BL/6J mice with NF-κB^{EGFP} mice (provided by Christian Jobin, University of North Carolina, Chapel Hill, North Carolina, USA) (83). These mice were then bred with *Ercc1*$^{+/-}$ FVB/n mice to generate *Ercc1*$^{-/-}$NF-κB^{EGFP} mice. *p65*$^{+/-}$ mice were bred with *Ercc1*$^{+/-}$ C57BL/6J mice. These were then bred with *Ercc1*$^{+/\Delta}$ FVB/n mice to generate *Ercc1*$^{-/\Delta}$*p65*$^{+/-}$ mice.

Isolation and treatment of MEFs. Double heterozygous mice were bred to yield WT, *Ercc1*$^{-/-}$, *Ercc1*$^{-/-}$*p65*$^{+/-}$, and *Ercc1*$^{-/-}$*p65*$^{-/-}$ pups for isolation of primary MEFs as previously described (45). The cells were grown in 1:1 DMEM/Ham's F10 supplemented with 10% FBS, 1%, penicillin and streptomycin, and 1% nonessential amino acids. They were passaged 5 times at 20% oxygen prior to fractionation using the NE-PER Cytoplasmic and Nuclear Extraction Reagent Kit (ThermoFisher Scientific) for Western blot analysis or EMSA. For 8K-NBD treatment, cells were incubated with 200 μM 8K-NBD for 3 hours prior to collection and immunoblotting for p-p65.

Nuclear extracts and Western blotting. Immunodetection of activated NF-κB and IκB in nuclear and cytoplasmic cell fractions was performed as previously described (84) using anti–p-p65 (93H1; Cell Signaling Technology), anti–p-IκBα (5A5; Cell Signaling Technology), and anti-IκBα (sc371; Santa Cruz Biotechnology Inc.). Anti-lamin A/C (sc20681; Santa Cruz Biotechnology Inc.) and anti–β-actin (Abcam) antibodies were used as loading controls for the nuclear and cytoplasmic fractions, respectively. Immunodetection of p16^{INK4a} from liver extracts was performed using anti-p16^{INK4a} antibody (sc1207; Santa Cruz Biotechnology Inc.) with anti-tubulin (ab4074, Abcam) as a loading control. All primary antibodies were used at a 1:1,000 dilution and an overnight incubation at 4°C.

EMSA. EMSA was completed based on a modified protocol described in ref. 85. Briefly, nuclear cellular fractions were extracted from MEFs using the NE-PER Cytoplasmic and Nuclear Extraction Reagent Kit (ThermoFisher Scientific). Five μg of each extract was mixed with 2 μl of 5X Gel Shift Binding Buffer (Promega) and nuclease-free distilled water in a 9 μl final volume. This was followed by incubation with an a-^{32}P-deoxycytodine triphosphate–radiolabeled DNA probe containing the NF-κB–binding domain (MP Biomedicals). The design of the NF-κB probe was described previously (86). The oligonucleotide sequences are as follows, with the DNA binding sequence underlined: NF-κB template, 5′-CAGGGCTGGGGATTCCCCATCTCCACAGTTTCACTTC-3′; NF-κB annealing, 5′-GAAGTGAAACTGTGG-3′ (Integrated DNA Technologies Inc.). dNTPs used to fill the overhangs were added using DNA Polymerase I, Large (Klenow) Fragment (Invitrogen), and the reaction was purified using illustra MicroSpin G50 Columns (GE Healthcare). Probes were added at a count per minute of approximately 150,000 in 1 μl, followed by separation on a 6% nondenaturing polyacrylamide gel. For competition assays, 2 μl of 100 μg/ml antibodies against p65/RelA and p50 were added to nuclear extracts and incubated for 20 minutes, prior to the addition of the duplex oligonucleotide.

Fluorescent microscopy. To quantify NF-κB activity, EGFP expression was measured in tissues, using MetaMorph software (MDS Analytical Technologies). Five images (×20 magnification) were taken of each tissue analyzed for each mouse ($n = 6$ per genotype at each age), and the percentage of cells expressing EGFP was quantified based on tissue area. This was reported as the fold increase in the number of EGFP$^+$ cells above the average value for controls. Anti-GFAP (13-0300; Invitrogen) was used at a 1:250 dilution and incubated overnight at 4°C. Anti–p-H2AX (05-636 Millipore) was used at a 1:500 dilution and incubated overnight at 4°C. For lipofuscin analysis, 5 images (×40 magnification) were taken of liver sections from

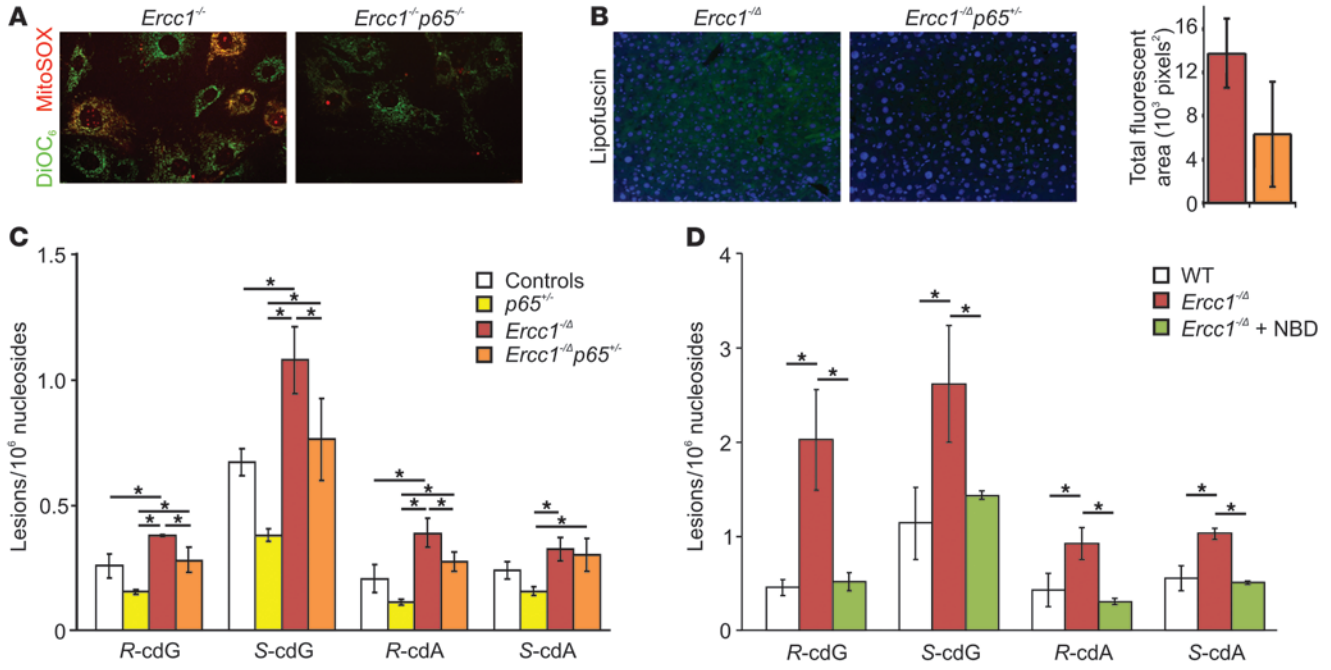

Figure 6

Inhibition of NF-κB reduces oxidative stress and damage in vitro and in vivo. (**A**) *Ercc1*$^{-/-}$ and *Ercc1*$^{-/-}$*p65*$^{-/-}$ passage 6 primary MEFs grown at 20% O_2 were stained with $DiOC_6$ (green) to mark mitochondria and MitoSOX (red) to detect mitochondrial superoxide anion (original magnification, ×40). (**B**) Liver sections from 10-week-old *Ercc1*$^{-/\Delta}$ and *Ercc1*$^{-/\Delta}$*p65*$^{+/-}$ mice imaged for lipofuscin fluorescence (original magnification, ×20). The histogram indicates the total fluorescent area for 5 images from 3 different mice per genotype calculated using MetaMorph software. (**C**) The levels of the (5′*R*) and (5′*S*) diastereomers of cdG and cdA in nuclear DNA isolated from the livers of 10-week-old control, *p65*$^{+/-}$, *Ercc1*$^{-/\Delta}$, and *Ercc1*$^{-/\Delta}$*p65*$^{+/-}$ mice. (**D**) The levels of cdG and cdA in nuclear DNA isolated from the livers of 19-week-old control, untreated *Ercc1*$^{-/\Delta}$, and 8K-NBD–treated *Ercc1*$^{-/\Delta}$ mice. **P* < 0.05, Tukey-Kramer test. Values denote the mean ± SEM (*n* = 3 per group).

control, *Ercc1*$^{-/\Delta}$, and *Ercc1*$^{-/\Delta}$*p65*$^{+/-}$ mice sacrificed at 10 weeks of age (*n* = 3 per genotype). To quantify lipofuscin, the total green fluorescent area was quantified using MetaMorph software. This was then reported as the average total area among the mice in the group.

Cell proliferation measurement. Proliferation was assessed as previously described (82). Briefly, WT and mutant MEFs were plated at a density of 0.25 × 10^6 MEFs per 6-cm dish. Cells were trypsinized at confluence, counted, and replated at the same density until mutant cells stopped growing. The total number of cells at each passage was calculated as follows: (no. of cells at previous passage/no. of cells plated) × no. of cells at current passage. The total cell number was plotted as the log cell number.

Senescence-associated β*-galactosidase*. Fixed liver sections from control, *Ercc1*$^{-/\Delta}$, and *Ercc1*$^{-/\Delta}$*p65*$^{+/-}$ mice sacrificed at 10 weeks of age (*n* > 9 per genotype) were stained for SA β-gal as described previously (87). Five images (×40 magnification) per mouse were taken on brightfield (SA β-gal), and DAPI staining was used to count total cell number per section. The percentage of cells that was senescent for each animal was averaged and plotted using SEM for error calculation.

Measurement of ROS in vitro. To measure superoxide anion levels, *Ercc1*$^{-/-}$*p65*$^{-/-}$ and *Ercc1*$^{-/-}$ MEFs were grown to 80%–90% confluency and rinsed with PBS. Media was replaced with serum-free media containing 5 μM MitoSOX reagent (M36008, Invitrogen) and 2.5 μM $DiOC_6$ (D273, Invitrogen). Cells were incubated for 25 minutes at 37°C. They were then washed twice with PBS, replaced with media containing serum, and imaged immediately.

Measurement of cPu in nuclear DNA of mouse livers. Nuclear DNA was isolated from mouse livers using a high-salt method (88) and analyzed for DNA damage as described previously (89). In brief, nuclear DNA was digested using a 4-enzyme cocktail, and uniformly ^{15}N-labeled cdA and cdG were added to the digestion mixture. The resulting nucleoside mixture was subjected to off-line high-performance liquid chromatography separation for the enrichment of the lesions under study, following previously described procedures (89). The LC-MS/MS/MS experiments were conducted using an LTQ linear ion trap mass spectrometer using recently described conditions (89).

Peptides. 8K-NBD (KKKKKKKKGGTALDWSWLQTE) and 8K-mNBD (KKKKKKKKGGTALDASALQTE), with the Trp to Ala substitutions designed to render the peptide inactive underlined, were synthesized at the University of Pittsburgh Peptide facility. Peptides were dissolved in DMSO at 40 μM and stored at –80°C until dilution in PBS directly before use.

NBD treatment of animals. Sibling pairs of *Ercc1*$^{-/\Delta}$ mice housed in a single cage were treated with 10 mg/kg 8K-NBD or 8K-mNBD 3 times per week i.p. by an investigator blinded as to the treatment group. Treatment began at 5 weeks of age, before the animals were symptomatic, and continued throughout their life span. Mice were euthanized via CO_2 inhalation at 12 or 18–20 weeks of age, and tissues were isolated for histopathological analysis.

Phenotype and weight measurements. Mice were weighed biweekly and assessed for the onset of characteristic progeroid symptoms, including kyphosis, dystonia, trembling, ataxia, and urinary incontinence due to neurodegeneration, and muscle wasting and reduced spontaneous activity due to frailty. The aging score is an overall measurement of the quality of life or healthspan and reflects the fraction of symptoms that occurred later in mice with reduced IKK/NF-κB activity. The aging score was determined as follows. For each symptom, the mouse in which the symptom was delayed received a score of +1 and the control littermate received a score of 0. If

the symptoms occurred simultaneously in both mice, both mice received score of 0. The sum of scores for each animal was divided by the number of symptoms measured to determine the fraction of symptoms delayed. This number was plotted for each animal and the average was determined for each treatment group to give an overall aging score.

Immunohistochemistry. Tissues were fixed in 10% formalin overnight, embedded in paraffin, and sectioned using a microtome by standard procedures. H&E staining was done according to standard procedures. Fixed frozen sections of liver were stained with oil red O by the following procedure. Slides were rinsed in running tap water for 10 minutes, rinsed with 60% isopropanol, stained with oil red O for 15 minutes, rinsed with 60% isopropanol, counterstained by dipping 15 times in hematoxylin, rinsed with distilled water, and mounted with gelvatol.

μCT. μCT of spines isolated from WT and *Ercc1*$^{-/\Delta}$ mice littermates was acquired using a VivaCT 40 (Scanco USA Inc.) with 15-μm isotropic voxel size resolution, 55 kVp of energy, and 145 μA of current. After the acquisition of transverse 2-dimensional image slices, 3-dimensional reconstruction of the lumbar vertebrae was performed using a constant threshold value of 235, which was selected manually for the bone voxels by visually matching the threshold areas to the gray-scale images.

Microarray. Genome-wide expression was measured in mice treated with 8K-NBD or 8K-mNBD as previously described (45, 47). All significant gene entries were subjected to GO classification (http://www.geneontology.org/). Significant overrepresentation of pathways and gene networks was determined by DAVID (http://david.abcc.ncifcrf.gov/summary.jsp; through BBID, BIOCARTA, and KEGG annotations) as well as by the ingenuity pathway analysis software (http://www.ingenuity.com/). The microarray data are available on ArrayExpress (E-MEXP-3615).

Statistics. To determine significance, a 2-tailed Student's *t* test was used, with *P* values of less than 0.05 considered significant. In addition, higher levels of significance ($P < 0.01$; $P < 0.001$) are indicated in Supplemental Table 1. For analysis of experiments involving more than 2 groups, ANOVA with a post-hoc Tukey-Kramer test was performed to determine significance (90). For the microarray data, significant overrepresentation of pathways and gene networks was determined by DAVID (http://david.abcc.ncifcrf.gov/summary.jsp) through BBID, BIOCARTA, and KEGG annotations, as well as by the ingenuity pathway analysis software (http://www.ingenuity.com/).

Study approval. Experiments involving mice were reviewed and approved by the University of Pittsburgh (Pittsburgh, Pennsylvania, USA) Institutional Animal Care and Use Committee and were in accordance with the NIH guidelines for the humane care of animals.

Acknowledgments

The authors would like to thank Irene Kamileri for assistance with the qPCR validation of microarray expression profiles, J.H.J. Hoeijmakers for providing reagents, and Christian Jobin for the NF-κB^{EGFP} reporter mice. This work was supported by NIH grants AG024827 and AR051456 to P.D. Robbins, CA101864 and ES019873 to Y. Wang, AG033907 to J. Huard, AG033046 to N. Vo, and ES016114 and CA103730 as well as a grant from the Ellison Medical Foundation (AG-NS-0303-05) to L.J. Niedernhofer. J.S. Tilstra was supported by NRSA grant AG032816. C.L. Clauson was supported by a Biomedical Research Fellowship from the Hartwell Foundation. This project used the University of Pittsburgh Cancer Institute Cell and Tissue Imaging and Animal Facilities and was supported in part by NIH award P30CA047904 and the NSRF 2007-2013 Cooperation EDGE 901-13/11/2009 to G.A. Garinis. The authors take full responsibility for the contents of this paper, which do not represent the NIH, the Department of Veterans Affairs, or the United States Government.

Received for publication November 15, 2010, and accepted in revised form May 10, 2012.

Address correspondence to: Paul D. Robbins or Laura J. Niedernhofer, Department of Metabolism and Aging, The Scripps Research Institute-Florida, 130 Scripps Way, Jupiter, Florida 33458, USA. Phone: 561.228.2126; Fax: 561.228.2173; E-mail: probbins@scripps.edu (P.D. Robbins). Phone: 561.228.2142; Fax: 561.228.2174; E-mail: lniedern@scripps.edu (L.J. Niedernhofer).

Paul D. Robbins' present address is: Department of Metabolism and Aging, The Scripps Research Institute-Florida, Jupiter, Florida, USA.

Laura J. Niedernhofer's present address is: Department of Metabolism and Aging, The Scripps Research Institute-Florida, Jupiter, Florida, USA.

1. Resnick NM, Marcantonio ER. How should clinical care of the aged differ? *Lancet*. 1997; 350(9085):1157–1158.
2. Kirkwood TB. Understanding the odd science of aging. *Cell*. 2005;120(4):437–447.
3. Chung HY, et al. Molecular inflammation: underpinnings of aging and age-related diseases. *Ageing Res Rev*. 2009;8(1):18–30.
4. Green DR, Galluzzi L, Kroemer G. Mitochondria and the autophagy-inflammation-cell death axis in organismal aging. *Science*. 2011;333(6046):1109–1112.
5. Liu L, Trimarchi JR, Smith PJ, Keefe DL. Mitochondrial dysfunction leads to telomere attrition and genomic instability. *Aging Cell*. 2002;1(1):40–46.
6. Trifunovic A, et al. Premature ageing in mice expressing defective mitochondrial DNA polymerase. *Nature*. 2004;429(6990):417–423.
7. Lee AC, et al. Ras proteins induce senescence by altering the intracellular levels of reactive oxygen species. *J Biol Chem*. 1999;274(12):7936–7940.
8. Packer L, Fuehr K. Low oxygen concentration extends the lifespan of cultured human diploid cells. *Nature*. 1977;267(5610):423–425.
9. Franceschi C, et al. Inflammaging and anti-inflammaging: a systemic perspective on aging and longevity emerged from studies in humans. *Mech Ageing Dev*. 2007;128(1):92–105.
10. Gosselin K, Abbadie C. Involvement of Rel/NF-kappa B transcription factors in senescence. *Exp Gerontol*. 2003;38(11–12):1271–1283.
11. Lavasani M, et al. Muscle-derived stem/progenitor cell dysfunction limits healthspan and lifespan in a murine progeria model. *Nat Commun*. 2012;3:608.
12. Conboy IM, Conboy MJ, Wagers AJ, Girma ER, Weissman IL, Rando TA. Rejuvenation of aged progenitor cells by exposure to a young systemic environment. *Nature*. 2005;433(7027):760–764.
13. Villeda SA, et al. The ageing systemic milieu negatively regulates neurogenesis and cognitive function. *Nature*. 2011;477(7362):90–94.
14. Brack AS, et al. Increased Wnt signaling during aging alters muscle stem cell fate and increases fibrosis. *Science*. 2007;317(5839):807–810.
15. Rando TA, Chang HY. Aging, rejuvenation, and epigenetic reprogramming: resetting the aging clock. *Cell*. 2012;148(1–2):46–57.
16. Hayden MS, Ghosh S. Shared principles in NF-kappaB signaling. *Cell*. 2008;132(3):344–362.
17. Hayden MS, West AP, Ghosh S. NF-kappaB and the immune response. *Oncogene*. 2006;25(51):6758–6780.
18. Wullaert A, Heyninck K, Beyaert R. Mechanisms of crosstalk between TNF-induced NF-kappaB and JNK activation in hepatocytes. *Biochem Pharmacol*. 2006;72(9):1090–1101.
19. Ramana KV, Friedrich B, Srivastava S, Bhatnagar A, Srivastava SK. Activation of nuclear factor-kappaB by hyperglycemia in vascular smooth muscle cells is regulated by aldose reductase. *Diabetes*. 2004; 53(11):2910–2920.
20. Bubici C, Papa S, Dean K, Franzoso G. Mutual cross-talk between reactive oxygen species and nuclear factor-kappa B: molecular basis and biological significance. *Oncogene*. 2006;25(51):6731–6748.
21. Furia B, et al. Enhancement of nuclear factor-kappa B acetylation by coactivator p300 and HIV-1 Tat proteins. *J Biol Chem*. 2002;277(7):4973–4980.
22. Kriete A, et al. Cell autonomous expression of inflammatory genes in biologically aged fibroblasts associated with elevated NF-kappaB activity. *Immun Ageing*. 2008;5:5.
23. Adler AS, Sinha S, Kawahara TL, Zhang JY, Segal E, Chang HY. Motif module map reveals enforcement of aging by continual NF-kB activity. *Genes Dev*. 2007;21(24):3244–3257.
24. Helenius M, Hanninen M, Lehtinen SK, Salminen A. Changes associated with aging and replicative senescence in the regulation of transcription factor nuclear factor-kappa B. *Biochem J*. 1996;318(pt 2):603–608.

25. Korhonen P, Helenius M, Salminen A. Age-related changes in the regulation of transcription factor NF-kappa B in rat brain. *Neurosci Lett*. 1997;225(1):61–64.
26. Bregegere F, Milner Y, Friguet B. The ubiquitin-proteasome system at the crossroads of stress-response and ageing pathways: a handle for skin care? *Ageing Res Rev*. 2006;5(1):60–90.
27. Giardina C, Hubbard AK. Growing old with nuclear factor-kappaB. *Cell Stress Chaperones*. 2002; 7(2):207–212.
28. Xiao ZQ, Majumdar AP. Induction of transcriptional activity of AP-1 and NF-kappaB in the gastric mucosa during aging. *Am J Physiol Gastrointest Liver Physiol*. 2000;278(6):G855–G865.
29. Tilstra JS, Clauson CL, Niedernhofer LJ, Robbins PD. NF-kB in aging and disease. *Aging Dis*. 2011; 2(6):449–465.
30. Li H, Malhotra S, Kumar A. Nuclear factor-kappa B signaling in skeletal muscle atrophy. *J Mol Med (Berl)*. 2008;86(10):1113–1126.
31. Cai D, et al. IKKbeta/NF-kappaB activation causes severe muscle wasting in mice. *Cell*. 2004; 119(2):285–298.
32. Ghosh A, et al. Selective inhibition of NF-kappaB activation prevents dopaminergic neuronal loss in a mouse model of Parkinson's disease. *Proc Natl Acad Sci U S A*. 2007;104(47):18754–18759.
33. Cuaz-Perolin C, et al. Antiinflammatory and antiatherogenic effects of the NF-kappaB inhibitor acetyl-11-keto-beta-boswellic acid in LPS-challenged ApoE$^{-/-}$ mice. *Arterioscler Thromb Vasc Biol*. 2008;28(2):272–277.
34. Valen G. Signal transduction through nuclear factor kappa B in ischemia-reperfusion and heart failure. *Basic Res Cardiol*. 2004;99(1):1–7.
35. Tilstra J, Rehman KK, Hennon T, Plevy SE, Clemens P, Robbins PD. Protein transduction: identification, characterization and optimization. *Biochem Soc Trans*. 2007;35(pt 4):811–815.
36. Berenbaum F. Signaling transduction: target in osteoarthritis. *Curr Opin Rheumatol*. 2004; 16(5):616–622.
37. Yamamoto Y, Gaynor RB. Role of the NF-kappaB pathway in the pathogenesis of human disease states. *Curr Mol Med*. 2001;1(3):287–296.
38. Kim HJ, et al. Antioxidant alpha-lipoic acid inhibits osteoclast differentiation by reducing nuclear factor-kappaB DNA binding and prevents in vivo bone resorption induced by receptor activator of nuclear factor-kappaB ligand and tumor necrosis factor-alpha. *Free Radic Biol Med*. 2006;40(9):1483–1493.
39. Karin M. Nuclear factor-kappaB in cancer development and progression. *Nature*. 2006; 441(7092):431–436.
40. Kawahara TL, et al. SIRT6 links histone H3 lysine 9 deacetylation to NF-kappaB-dependent gene expression and organismal life span. *Cell*. 2009; 136(1):62–74.
41. Mostoslavsky R, et al. Genomic instability and aging-like phenotype in the absence of mammalian SIRT6. *Cell*. 2006;124(2):315–329.
42. Natoli G. When sirtuins and NF-kappaB collide. *Cell*. 2009;136(1):19–21.
43. Goss JR, et al. Premature aging-related peripheral neuropathy in a mouse model of progeria. *Mech Ageing Dev*. 2011;132(8–9):437–442.
44. Gregg S, et al. A mouse model of accelerated liver aging due to a defect in DNA repair. *Hepatology*. 2012; 55(2):609–621.
45. Niedernhofer LJ, et al. A new progeroid syndrome reveals that genotoxic stress suppresses the somatotroph axis. *Nature*. 2006;444(7122):1038–1043.
46. Vo N, et al. Accelerated aging of intervertebral discs in a mouse model of progeria. *J Orthop Res*. 2010; 28(12):1600–1607.
47. Schumacher B, et al. Delayed and accelerated aging share common longevity assurance mechanisms. *PloS Genet*. 2008;4(8):e1000161.
48. Magness ST, Jijon H, Van Houten Fisher N, Sharpless NE, Brenner DA, Jobin C. In vivo pattern of lipopolysaccharide and anti-CD3-induced NF-kappa B activation using a novel gene-targeted enhanced GFP reporter gene mouse. *J Immunol*. 2004; 173(3):1561–1570.
49. Dollé M, et al. Broad segmental progeroid changes in short-lived *Ercc1*$^{-/\Delta 7}$ mice. *Pathobiology Of Aging and Age-Related Diseases, 1*. doi:10.3402/pba.v1i0.7219. 2011.
50. Farrell GC, Larter CZ. Nonalcoholic fatty liver disease: from steatosis to cirrhosis. *Hepatology*. 2006;43(2 suppl 1):S99–S112.
51. Remuzzi A, et al. Effect of angiotensin II antagonism on the regression of kidney disease in the rat. *Kidney Int*. 2002;62(3):885–894.
52. Rodriguez-Puyol D. The aging kidney. *Kidney Int*. 1998;54(6):2247–2265.
53. Nichols NR, Day JR, Laping NJ, Johnson SA, Finch CE. GFAP mRNA increases with age in rat and human brain. *Neurobiol Aging*. 1993;14(5):421–429.
54. Acharyya S, et al. Interplay of IKK/NF-kappaB signaling in macrophages and myofibers promotes muscle degeneration in Duchenne muscular dystrophy. *J Clin Invest*. 2007;117(4):889–901.
55. Dave SH, et al. Amelioration of chronic murine colitis by peptide-mediated transduction of the IkappaB kinase inhibitor NEMO binding domain peptide. *J Immunol*. 2007;179(11):7852–7859.
56. Dai S, Hirayama T, Abbas S, Abu-Amer Y. The IkappaB kinase (IKK) inhibitor, NEMO-binding domain peptide, blocks osteoclastogenesis and bone erosion in inflammatory arthritis. *J Biol Chem*. 2004; 279(36):37219–37222.
57. Ghosh A, et al. Selective inhibition of NF-kappaB activation prevents dopaminergic neuronal loss in a mouse model of Parkinson's disease. *Proc Natl Acad Sci U S A*. 2007;104(47):18754–18759.
58. Parrinello S, Samper E, Krtolica A, Goldstein J, Melov S, Campisi J. Oxygen sensitivity severely limits the replicative lifespan of murine fibroblasts. *Nat Cell Biol*. 2003;5(8):741–747.
59. Rodier F, et al. DNA-SCARS: distinct nuclear structures that sustain damage-induced senescence growth arrest and inflammatory cytokine secretion. *J Cell Sci*. 2011;124(pt 1):68–81.
60. Rodier F, Campisi J. Four faces of cellular senescence. *J Cell Biol*. 2011;192(4):547–556.
61. Taubold RD. Studies on chemical nature of lipofusion (age pigment) isolated from normal human brain. *Lipids*. 1975;10(7):383–390.
62. Tappel AL. Lipid peroxidation damage to cell components. *Fed Proc*. 1973;32(8):1870–1874.
63. Siakotos AN, Koppang N. Procedures for the isolation of lipopigments from brain, heart and liver, and their properties: A review. *Mech Ageing Dev*. 1973; 2(3):177–200.
64. Fletcher BL, Dillard CJ, Tappel AL. Measurement of fluorescent lipid peroxidation products in biological systems and tissues. *Anal Biochem*. 1973;52(1):1–9.
65. Jaruga P, Dizdaroglu M. 8,5′-Cyclopurine-2′-deoxynucleosides in DNA: Mechanisms of formation, measurement, repair and biological effects. *DNA Repair*. 2008;7(9):1413–1425.
66. Hasty P, Campisi J, Hoeijmakers J, van Steeg H, Vijg J. Aging and genome maintenance: lessons from the mouse? *Science*. 2003;299(5611):1355–1359.
67. Gregg SQ, Robinson AR, Niedernhofer LJ. Physiological consequences of defects in ERCC1-XPF DNA repair endonuclease. *DNA Repair*. 2011; 10(7):781–791.
68. Miyamoto S. Nuclear initiated NF-[kappa]B signaling: NEMO and ATM take center stage. *Cell Res*. 2011;21(1):116–130.
69. Lim W, Cho J, Kwon HY, Park Y, Rhyu MR, Lee Y. Hypoxia-inducible factor 1 alpha activates and is inhibited by unoccupied estrogen receptor beta. *FEBS Lett*. 2009;583(8):1314–1318.
70. Shtutman M, et al. The cyclin D1 gene is a target of the beta-catenin/LEF-1 pathway. *Proc Natl Acad Sci U S A*. 1999;96(10):5522–5527.
71. Li Y, et al. Regulation of FOXO3a/beta-catenin/GSK-3beta signaling by 3,3′-diindolylmethane contributes to inhibition of cell proliferation and induction of apoptosis in prostate cancer cells. *J Biol Chem*. 2007;282(29):21542–21550.
72. Scheidereit C. IkappaB kinase complexes: gateways to NF-kappaB activation and transcription. *Oncogene*. 2006;25(51):6685–6705.
73. Harrison DE, et al. Rapamycin fed late in life extends lifespan in genetically heterogeneous mice. *Nature*. 2009;460(7253):392–395.
74. Selman C, et al. Ribosomal protein S6 kinase 1 signaling regulates mammalian life span. *Science*. 2009; 326(5949):140–144.
75. Dan HC, Cooper MJ, Cogswell PC, Duncan JA, Ting JP, Baldwin AS. Akt-dependent regulation of NF-{kappa}B is controlled by mTOR and Raptor in association with IKK. *Genes Dev*. 2008;22(11):1490–1500.
76. Baur JA, et al. Resveratrol improves health and survival of mice on a high-calorie diet. *Nature*. 2006; 444(7117):337–342.
77. Gilmore T. Rel/NF-kB transcription factors. Boston University Web site. www.nf-kb.org. Accessed May 10, 2012.
78. Jackson JG, Pereira-Smith OM. p53 is preferentially recruited to the promoters of growth arrest genes p21 and GADD45 during replicative senescence of normal human fibroblasts. *Cancer Res*. 2006; 66(17):8356–8360.
79. Provost PR, Marcel YL, Milne RW, Weech PK, Rassart E. Apolipoprotein D transcription occurs specifically in nonproliferating quiescent and senescent fibroblast cultures. *FEBS Letters*. 1991;290(1–2):139–141.
80. Coppe JP, et al. Senescence-associated secretory phenotypes reveal cell-nonautonomous functions of oncogenic RAS and the p53 tumor suppressor. *PLoS Biol*. 2008;6(12):2853–2868.
81. Baker DJ, et al. Clearance of p16Ink4a-positive senescent cells delays ageing-associated disorders. *Nature*. 2011;479(7372):232–236.
82. Ahmad A, et al. ERCC1-XPF endonuclease facilitates DNA double-strand break repair. *Mol Cell Biol*. 2008;28(16):5082–5092.
83. Karrasch T, Kim JS, Muhlbauer M, Magness ST, Jobin C. Gnotobiotic IL-10-/-;NF-kappa B(EGFP) mice reveal the critical role of TLR/NF-kappa B signaling in commensal bacteria-induced colitis. *J Immunol*. 2007;178(10):6522–6532.
84. Xiong H, et al. Inhibition of interleukin-12 p40 transcription and NF-kappaB activation by nitric oxide in murine macrophages and dendritic cells. *J Biol Chem*. 2004;279(11):10776–10783.
85. Reay DP, et al. Systemic delivery of NEMO binding domain/IKKgamma inhibitory peptide to young mdx mice improves dystrophic skeletal muscle histopathology. *Neurobiol Dis*. 2011;43(3):598–608.
86. Guttridge DC, Albanese C, Reuther JY, Pestell RG, Baldwin AS Jr. NF-kappaB controls cell growth and differentiation through transcriptional regulation of cyclin D1. *Mol Cell Biol*. 1999;19(8):5785–5799.
87. Debacq-Chainiaux F, Erusalimsky JD, Campisi J, Toussaint O. Protocols to detect senescence-associated beta-galactosidase (SA-betagal) activity, a biomarker of senescent cells in culture and in vivo. *Nat Protoc*. 2009;4(12):1798–1806.
88. Miller SA, Dykes DD, Polesky HF. A simple salting out procedure for extracting DNA from human nucleated cells. *Nucleic Acids Res*. 1988;16(3):1215.
89. Wang J, Yuan B, Guerrero C, Bahde R, Gupta S, Wang Y. Quantification of oxidative DNA lesions in tissues of Long-Evans Cinnamon rats by capillary high-performance liquid chromatography-tandem mass spectrometry coupled with stable isotope-dilution method. *Anal Chem*. 2011;83(6):2201–2209.
90. McDonald JH. *Handbook of Biological Statistics*. 2nd ed. Baltimore, Maryland, USA: Sparky House Publishing; 2009.